Jerzy BOBIŃSKI*, Jacek TEJCHMAN*

# SIMULATIONS OF FRACTURE IN CONCRETE ELEMENTS USING CONTINUOUS AND DISCONTINUOUS MODELS

*SUMMARY*

*The paper presents results of numerical simulations of fracture in concrete using two different approaches. First, fracture was modelled in a smeared way by an elasto-plastic and a damage continuum model. In elasto-plasticity, a Rankine criterion was used. The degradation of the stiffness in the damage model was described as a scalar variable of an equivalent strain measure. To ensure mesh-independent results, a non-local theory was used. Second, fracture was simulated as discontinuities with the aid of cohesive elements and Extended Finite Element Method (XFEM). The experimental benchmark test for concrete by Nooru-Mohamed under mixed mode conditions was modelled. The obtained numerical results were compared with the corresponding experimental ones.*

***Keywords****: concrete, non-locality, plasticity, damage mechanics, XFEM*

*SYMULACJE ZARYSOWANIA W ELEMENTACH BETONOWYCH Z ZASTOSOWANIEM PODEJŚCIA CIĄGŁEGO I NIECIĄGŁEGO*

*W pracy przedstawiono wyniki symulacji numerycznych MES pękania w betonie z wykorzystaniem dwóch różnych podejść. Po pierwsze, zastosowano ciągły (przesmarowany) opis rys w teorii plastyczności oraz model degradacji modułu sprężystości z różnymi opisami odkształcenia zastępczego w ramach kontynualnej mechaniki uszkodzeń. Oba prawa rozszerzono o długość charakterystyczną mikrostruktury w ramach teorii nielokalnej w celu uzyskania wyników niezależnych od siatki MES. Po drugie, jako alternatywę do symulacji propagacji rys zastosowano nieciągły opis pola przemieszczeń, wykorzystując elementy kohezyjne oraz rozszerzoną metodę elementów skończonych XFEM. Przeprowadzono symulacje numeryczne testu Nooru–Mohamada z jednoczesnym rozciąganiem i ścinaniem betonu. Uzyskane wyniki numeryczne porównano z wynikami doświadczalnymi.*

***Słowa kluczowe****: beton, nielokalność, plastyczność, kontynualna mechanika uszkodzeń, XFEM*

## 1. INTRODUCTION

Fracture process is a fundamental phenomenon in quasi-brittle materials like concrete. At the beginning of the loading, regions with several micro-cracks are formed. Later these micro-cracks create macro-cracks. Thus, a fracture process is subdivided in general into 2 main stages: appearance of narrow regions of intense deformation (including micro-cracks) and occurrence of macro-cracks. Within continuum mechanics, strain localization can be numerically captured by a continuous approach and discrete macro-cracks by a discontinuous one. Usually, to describe the fracture behaviour of concrete, one approach is used. However, in order to describe the entire fracture process, a continuous approach should be connected with a discontinuous one [1].

Using a continuous approach, strain localization can be described using e.g. elasto-plastic, damage mechanics or coupled constitutive models. These formulations include softening, so they have to be equipped with a characteristic length of the microstructure to preserve the well-posedness of the boundary value problem. The length can be introduced by means of a micro-polar [2], non-local [3] or gradient theory [4]. Alternatively, fracture is described by discrete macro-cracks with a displacement jump (by omitting a micro-crack phase). The oldest solutions used interface elements defined along element edges. The modern ones allow now for considering cracks in the interior of finite elements with embedded discontinuities or by using the Extended Finite Element Method XFEM based on the partition of unity concept [5], which adds global degrees of freedom at nodes to describe jumps in a displacement field. This technique was originally used to simulate brittle materials [6, 7] and next it was extended to simulate cracks in quasi-brittle materials [8].

To validate the constitutive approaches to simulate fracture, benchmark tests are used. One of the most popular benchmarks for plain concrete is the so-called Nooru–Mohamed test [9], which considers the concrete behaviour under simultaneous tension and shear. The numerical simulations of this test have been already performed with elasto-plastic laws [10, 11], damage mechanics [12, 13], strong discontinuities [14, 15] and lattice models [16, 17].

The main aim of the paper is to check the ability of different numerical approaches to simulate curved cracks in plain concrete appearing during the Nooru–Mohamed test [9]. First, two continuum constitutive laws based on an elasto-plasticity and a damage theory were applied. Later, two continuum models treating fracture in a discrete way were used. All models properly regularize boundary value problems involving cracks [18].

* Politechnika Gdańska

The paper is organised as follows. Section 2 describes continuum constitutive laws, while Section 3 introduces a non-local theory used to regularize continuum models. Discontinuous formulations for concrete are presented in Section 4. The FE results are described and discussed in Section 5. Finally, Section 6 includes some conclusions.

## 2. CONTINUUM CONSTITUTIVE MODELS

### 2.1. Elasto-plasticity

The Rankine's criterion was used with the yield function $f$ defined as

$$f = \max\{\sigma_1, \sigma_2, \sigma_3\} - \sigma_t(\kappa) \tag{1}$$

where:

$\sigma_1$, $\sigma_2$ and $\sigma_3$ – the principal stresses,
$\sigma_t$ – the tensile yield stress,
$\kappa$ – the hardening/softening parameter (equal to the maximum principal plastic strain $\varepsilon_1^p$).

An associated flow rule was assumed. In plane stress simulations, the Rankine's criterion consists of two yield functions for $\sigma_1$ and $\sigma_2$ with two independent plastic multipliers at the same $\sigma_t$. To define softening under tension, a curve proposed by Hordijk [19] was applied

$$\sigma_t(\kappa) = f_t\left(\left(1+\frac{c_1}{\kappa_u}\kappa^3\right)\exp\left(-\frac{c_2}{\kappa_u}\kappa\right) - \left(1+c_1^3\right)\exp(-c_2)\frac{\kappa}{\kappa_u}\right) \tag{2}$$

with $\kappa_u$ as the ultimate value of the softening parameter $\kappa$ ($c_1 = 3.0$ and $c_2 = 6.93$).

### 2.2. Damage mechanics

The material damage was described by a scalar parameter $D$ growing from zero (undamaged) to one (total damage) and acting as a stiffness reduction factor:

$$\sigma_{ij} = (1-D)C^e_{ijkl}\varepsilon_{kl} \tag{3}$$

where $C^e_{ijkl}$ is the elastic stiffness matrix and $\varepsilon_{kl}$ denotes the total strain tensor. The growth of the variable $D$ was controlled by a damage threshold parameter $\kappa$ which was defined as the maximum of the equivalent strain measure $\tilde{\varepsilon}$ reached during the entire load history:

$$\kappa(t) = \max_{\tau \le t}\{\tilde{\varepsilon}(\tau)\} \tag{4}$$

During loading, the parameter $\kappa$ increases, and during unloading and reloading, it remains constant. To describe the evolution of the damage variable $D$, an exponential softening law was used:

$$D = 1 - \frac{\kappa_0}{\kappa}\left(1 - \alpha + \alpha e^{-\beta(\kappa-\kappa_0)}\right) \tag{5}$$

wherein:

$\kappa_0$ – the initial value of the damage threshold parameter $\kappa$,
$\alpha$ and $\beta$ – the material parameters.

Several definitions of the equivalent strain measure $\tilde{\varepsilon}$ were tested.

First, a modified von Mises definition [20] in terms of strains was used:

$$\tilde{\varepsilon} = \frac{k-1}{2k(1-2\nu)}I_1 + \frac{1}{2k}\sqrt{\left(\frac{k-1}{1-2\nu}I_1^{\varepsilon}\right)^2 + \frac{12k}{(1+\nu)^2}J_2^{\varepsilon}} \tag{6}$$

where $I_1^{\varepsilon}$ and $J_2^{\varepsilon}$ are the first invariant of the strain tensor and second invariant of the deviatoric strain tensor, respectively:

$$I_1^{\varepsilon} = \varepsilon_{11} + \varepsilon_{22} + \varepsilon_{33} \quad \text{and} \quad J_{21}^{\varepsilon} = \frac{1}{2}\varepsilon_{ij}\varepsilon_{ij} - \frac{1}{6}\left(I_1^{\varepsilon}\right)^2 \tag{7}$$

The parameter $k$ in Eqn. (6) denotes the ratio between the compressive and tensile strength of the material.

Second, the so-called Rankine definition [21] was used:

$$\tilde{\varepsilon} = \frac{\max\left\{\sigma_i^{eff}\right\}}{E} \tag{8}$$

where:

$E$ – the modulus of elasticity,
$\sigma_i^{eff}$ – the principal values of the effective stress tensor defined as:

$$\sigma_{ij}^{eff} = C^e_{ijkl}\varepsilon_{kl} \tag{9}$$

Finally, we used a formula proposed by Häuβler-Combe and Prochtel [22] based on the failure surface for concrete formulated by Hsieh *et al*. [23]. The equivalent strain measure was calculated as [24]:

$$\tilde{\varepsilon} = \frac{1}{2}\left(c_2\sqrt{J_2^{\varepsilon}} + c_3\varepsilon_1 + c_4 I_2^{\varepsilon} + \sqrt{\left(c_2\sqrt{J_2^{\varepsilon}} + c_3\varepsilon_1 + c_4 I_2^{\varepsilon}\right)^2 + 4c_1 J_2^{\varepsilon}}\right) \tag{10}$$

with the constants $c_1$, $c_2$, $c_3$ and $c_4$ depending on the ratio $\alpha_1$ between strengths in uniaxial compression and tension ($\alpha_1 = f_t/f_c = k$), the ratio $\alpha_2$ between the biaxial and uniaxial strength in compression ($\alpha_2 = f_{bc}/f_c$) and the ratios $\alpha_3$ and $\gamma$ from triaxial compression ($\sigma_1 = \sigma_2 = -\gamma f_c$, $\sigma_3 = -\alpha_3 f_c$).

## 3. NON-LOCAL THEORY

As a regularization technique for continuum constitutive models, a non-local theory was used. It is based on a spatial averaging of tensor or scalar state variables in a certain neighbourhood of a given point. In plasticity, rates of the softening parameters $d\kappa$ were treated non-locally according to the Brinkgreve's [25] proposal:

$$d\bar{\kappa}(\mathbf{x}) = (1-m)\,d\kappa(\mathbf{x}) + m\frac{\int_V \alpha_0\left(\|\mathbf{x}-\boldsymbol{\xi}\|\right) d\kappa(\boldsymbol{\xi})\,d\boldsymbol{\xi}}{\int_V \alpha_0\left(\|\mathbf{x}-\boldsymbol{\xi}\|\right) d\boldsymbol{\xi}} \tag{11}$$

where:

- $V$ – volume,
- $\bar{\kappa}$ – the non-local softening parameter,
- $m$ – the coefficient greater than one (note that the classical averaging formula with $m = 1$ does not ensure mesh-independent results [25]),
- $\boldsymbol{x}$ – the coordinates of the considered (actual) point,
- $\boldsymbol{\xi}$ – the coordinates of the surrounding points,
- $\alpha_0$ – the weighting function.

As the weighting function $\alpha_0$, the Gauss distribution was assumed:

$$\alpha_0(r) = \frac{1}{l\sqrt{\pi}} e^{-\left(\frac{r}{l}\right)^2} \tag{12}$$

where:

- $r = \|\boldsymbol{x}-\boldsymbol{\xi}\|$ – the distance between points $\boldsymbol{x}$ and $\boldsymbol{\xi}$,
- $l$ – the characteristic length of microstructure.

It should be noted that the averaging was restricted only to a small area around each material point; the influence of points at the distance of $r = 3\times l$ was only of 0.01%.

In a damage model, a local definition of the equivalent strain measure $\tilde{\varepsilon}$ from Eqs. (6), (8) and (10) was replaced in Eqn. (4) by its non-local counterpart $\bar{\varepsilon}$:

$$\bar{\varepsilon}(\boldsymbol{x}) = \frac{\int_V \alpha_0\left(\|\boldsymbol{x}-\boldsymbol{\xi}\|\right)\tilde{\varepsilon}(\boldsymbol{\xi})\,d\boldsymbol{\xi}}{\int_V \alpha_0\left(\|\boldsymbol{x}-\boldsymbol{\xi}\|\right) d\boldsymbol{\xi}} \tag{13}$$

## 4. DISCRETE CONSTITUTIVE MODELS

### 4.1. Interface cohesive elements

Interface elements were defined along edges of continuum finite elements (bulk elements) to simulate crack nucleation and growth. The bulk elements were modelled as linear elastic ones. Interface elements were equipped with irreversible cohesive laws to simulate the separation of crack faces. A simple damage constitutive relationship between the traction vector $\boldsymbol{t}$ and separation/displacement jump vector $[[\boldsymbol{u}]]$ (both quantities with normal and shear terms) was assumed:

$$t = (1-D)E_0\boldsymbol{I}[[\boldsymbol{u}]] \tag{14}$$

with the penalty (dummy) stiffness $E_0$ and unit tensor $\boldsymbol{I}$. To take into account both the normal and shear terms in the separation vector, the effective displacement was introduced [26]:

$$\delta_{eff} = \sqrt{\langle\delta_n\rangle^2 + \eta\delta_s^2} \tag{15}$$

with the coefficient $\eta$. To describe softening after cracking, an exponential law was assumed [26]:

$$\sigma_t(\delta_{\max}) = f_t \exp\left(-\beta\left(\delta_{\max} - \frac{f_t}{E_0}\right)\right) \tag{16}$$

with

$$\delta_{\max} = \max_{\tau\le t}\delta_{eff}(\tau)$$

where $\beta$ is the parameter describing the slope of the softening curve.

### 4.2. Extended Finite Element Method (XFEM)

The Extended Finite Element Method, based on the Partition of Unity (PUM) [5], enables adding locally extra terms to a standard FE displacement field approximation in order to capture displacement discontinuities. These extra terms are defined based on a known analytical solution of the problem. The key idea is to enrich only selected nodes with additional degrees of freedom.

In problems where tension dominates, we assumed a linear elastic constitutive law in uncracked continuum in XFEM due to a linear relationship between tensile strains and stresses occurring in concrete almost up to the peak. Moreover crack tip can be placed only at element edges. To activate (create or extend) a crack, the Rankine condition has to be fulfilled in integration points of the element at the front of the crack tip:

$$\max\{\sigma_1,\sigma_2,\sigma_3\} > f_t \tag{17}$$

Usually, the crack is activated, if Eqn. (17) is fulfilled in any integration point in the element. For elements with more integration points, this condition seems to be the safest one; other solutions (e.g. $\sigma_1 > f_t$ in all integrations points) can overestimate the maximum load. The extension direction is perpendicular to the direction of the maximum

principal stress. To smooth the stress field around the crack tip, non-local stresses $\boldsymbol{\sigma}^*$ were taken to determine the crack direction [27]

$$\boldsymbol{\sigma}^* = \int_V \boldsymbol{\sigma} w dV \quad \text{and} \quad w = \frac{1}{(2\pi)^{3/2} \bar{l}^3} \exp\left(-\frac{r^2}{2\bar{l}^2}\right) \tag{18}$$

where the domain $V$ is the semicircle at the front of the crack tip, $w$ is the weighting function, $\bar{l}$ is the averaging length (usually equal to 3 times the average element size) and $r$ denotes the distance between the integration point and crack tip. The averaging length $\bar{l}$ is not connected to material microstructure (as the characteristic length $l$ in Eqn. (12)). A discrete cohesive law links tractions $\boldsymbol{t}$ with displacement jumps $[[\boldsymbol{u}]]$ at the discontinuity. We assumed the simplest loading function:

$$f\left([[u_n]], \kappa\right) = [[u_n]] - \kappa \tag{19}$$

with the history parameter $\kappa$ equal to the maximum value of the normal displacement jump $[[u_n]]$ achieved during loading. Softening of the normal component of traction vector was described using an exponential formula:

$$t_n = f_t \exp\left(-\frac{f_t \kappa}{G_f}\right) \tag{20}$$

where $G_f$ – the fracture energy. During unloading, the secant stiffness is used with a return to the origin (damage format). In a compressive regime, a penalty elastic stiffness matrix is assumed. In a tangent direction, a linear relationship between a displacement jump and traction is defined with the stiffness $T_s$ in the first step (in contrast to the cohesive crack model of Section 4.1).

## 5. NUMERICAL RESULTS

A double-edge notched (DEN) concrete specimen under various different loading paths of combined shear and tension was analysed. Originally it was experimentally examined by Nooru–Mohamed [9]. The dimensions of the largest specimen and boundary conditions are presented in Figure 1.

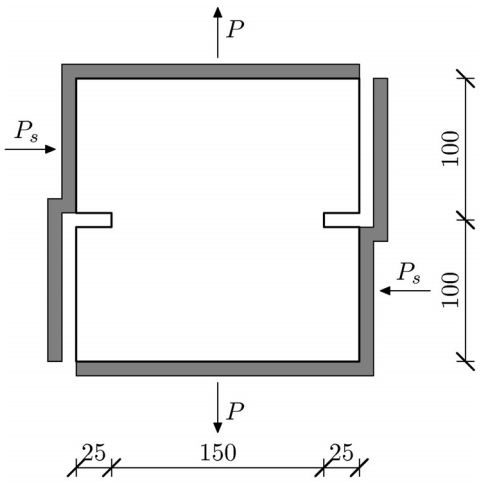


**Fig. 1.** Experiment by Nooru–Mohamed [9]

The length and height of the element were 200 mm. The thickness was 50 mm. Two notches with dimensions of 25×5 mm$^2$ were placed in the middle of the vertical edges. The loading was prescribed by rigid steel frames glued to concrete. During one of the loading paths (number '4'), a shear force $P_s$ was applied until it reached a specified value, while the horizontal edges were free. At the second stage, the shear force remained constant and vertical tensile displacement was prescribed. In the experiment, two curved cracks with an inclination depending upon the shear force were obtained (for a small value of $P_s$ – cracks were almost horizontal, for a large value of $P_s$ – cracks were strongly curved) (Fig. 2).

The elastic material parameters reported in [10] were chosen in the FE-analyses: $E$ = 32.8 GPa and $\nu$ = 0.2. A FE-mesh was composed of 3-node triangles or 4-node quadrilateral finite elements. The material parameters in softening were fitted with the experimental results. Therefore the different tensile strength and fracture energy were used (they did not influence the shape of cracks). Only for XFEM the tensile strength originally reported by Nooru–Mohamed [9] was used. Note that the tensile strength is always characterized by a large scatter. The maximum element size in the localized zone was about 1.5 mm. To prevent a crack creation near both left-lower and right-upper corners, a linear elastic material was defined in these regions. All simulations were performed under plane stress conditions.

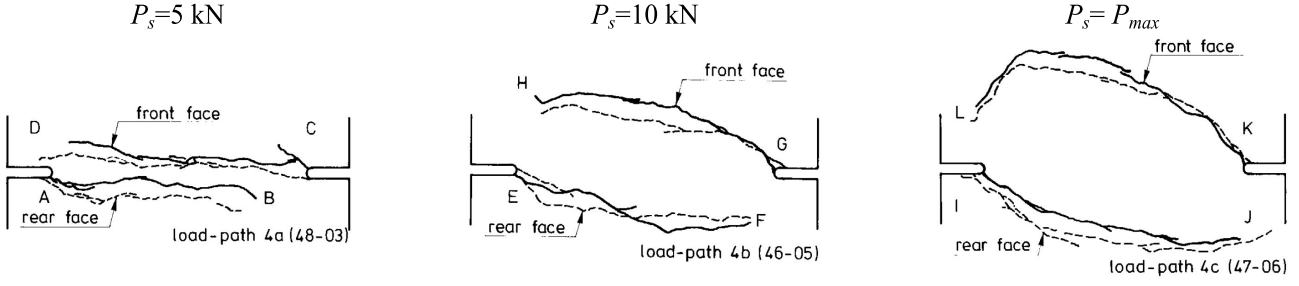


**Fig. 2.** Experimental crack patterns [9]

### 5.1. Elasto-plasticity

The tensile strength was assumed as $f_t$ = 2.4 MPa and the parameter $\kappa_u$ = 0.02. The characteristic length was equal to $l$ = 2 mm and the non-locality parameter was $m$ = 2. The FE-mesh consisted of about 8000 quadrilateral elements.

Figure 3 presents the obtained FE results with the horizontal shear force $P_s$ = 5 kN. A very good agreement was achieved with respect to both the force-displacement curve and strain localization ($\delta$ is the vertical displacement of the top edge), although the calculated maximum vertical force $P$ was slightly too high. In turn, the FE results for the path 4b ($P_s$ = 10 kN) are shown in Figure 4. The force-displacement curve is satisfactorily reproduced. Two curved localized zones were numerically obtained again, but they were too flat as compared to the experiment (wherein they were more curved and the distance between them was larger). Finally Figure 5 shows the FE-results with the experimental maximum shear force. In the experiment, this value was equal to 27.5 kN, however in the FE-simulations a smaller force (25.4 kN) was calculated. The crack pattern was in a moderate agreement with experiments; the cracks were curved at the end, but they were straight at the beginning. The force-displacement curves differed significantly, but compressive nature of the vertical force was well reproduced. The differences between the numerical and experimental results with respect to the initial stiffness can be explained by e.g. glued edges or frame stiffness of the experimental setup.

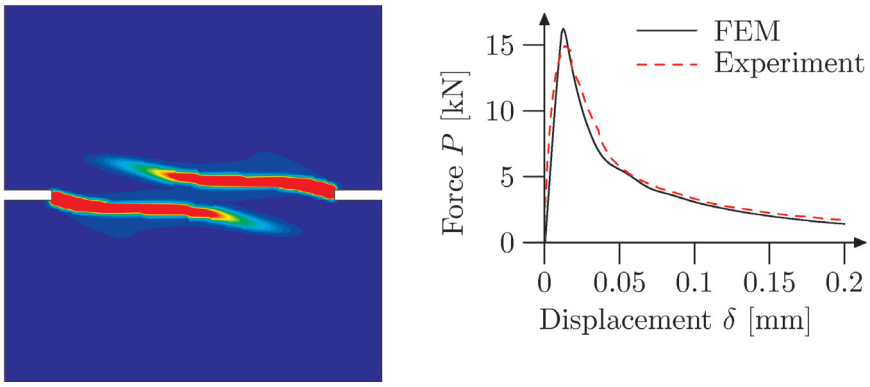


**Fig. 3.** Calculated contour map of non-local parameter $\bar{\kappa}$ and force-displacement curve at shear force $P_s$ = 5 kN using elasto-plasticity

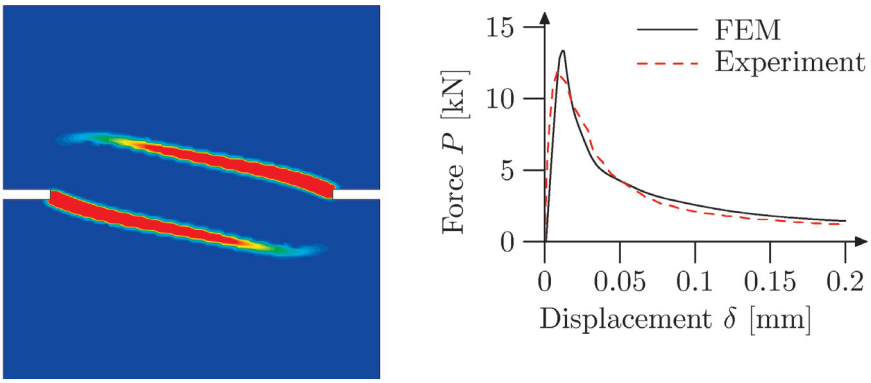


**Fig. 4.** Calculated contour map of non-local parameter $\bar{\kappa}$ and force-displacement curve at shear force $P_s$ = 10 kN using elasto-plasticity

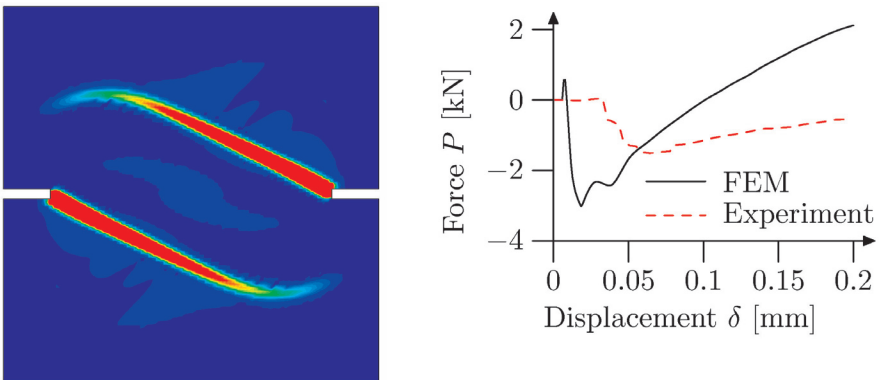


**Fig. 5.** Calculated contour map of non-local parameter $\bar{\kappa}$ and force-displacement curve at shear force $P_s$ = 25.4 kN using elasto-plasticity

### 5.2. Damage mechanics

The FE-mesh consisted again of about 8000 quadrilateral elements. First, the modified von Mises definition (Eqn. (6)) was used. The following material parameters were chosen: $l$ = 2 mm, $\kappa_0 = 7\times10^{-5}$, $\alpha$ = 0.92 and $\beta$ = 250. The coefficient $k$ was taken as 12.5. Figures 6–8 present the obtained FE results. The maximum allowable shear force was equal to 29.9 kN (higher than in the experiment). At all levels of the shear force, two curved cracks were reproduced, although too curved as compared to experiments. A very good agreement was obtained in force-displacement diagrams at $P_s$ = 5 kN and $P_s$ = 10 kN. For the maximum shear force, some differences occurred, but the compressive character of the vertical force was again captured.

Next, the Rankine definition of the equivalent strain measure $\tilde{\varepsilon}$ (Eqn. (8)) was tested. The material parameters were taken as: $\kappa_0 = 7\times10^{-5}$, $\alpha$ = 0.92, $\beta$ = 200 and $l$ = 2 mm. For the shear forces 5 kN and 10 kN only one crack between notches was created and a sudden drop after the peak occurred in force-displacements diagrams (Figs. 9 and 10). At the maximum shear force equal to 25.3 kN, surprisingly satisfactory results were recovered (Fig. 11).

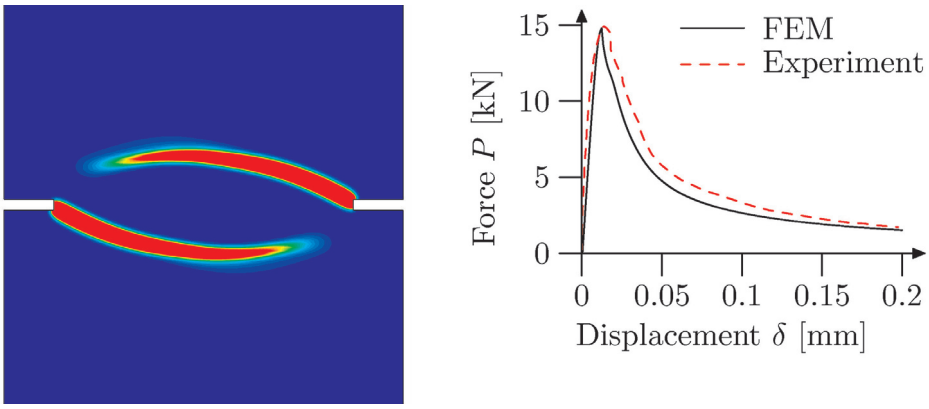


**Fig. 6.** Calculated contour map of parameter $\kappa$ and force-displacement curve at shear force $P_s$ = 5 kN using damage mechanics with Eqn. (6)

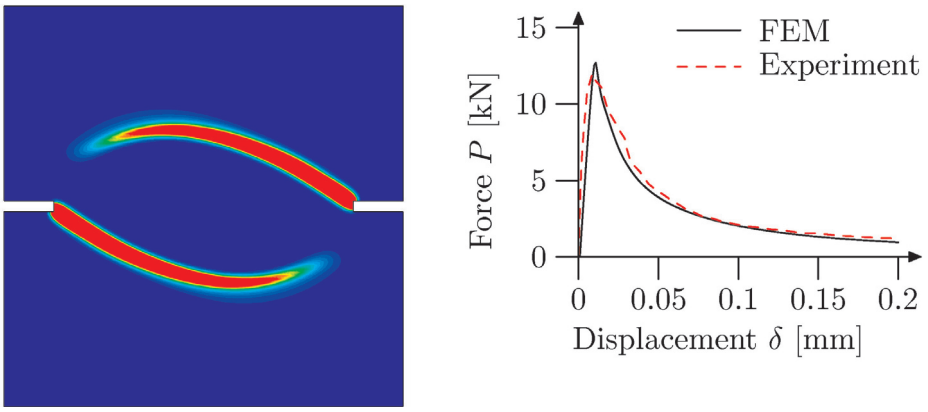


**Fig. 7.** Calculated contour map of parameter $\kappa$ and force-displacement curve at shear force $P_s$ = 10 kN using damage mechanics with Eqn. (6)

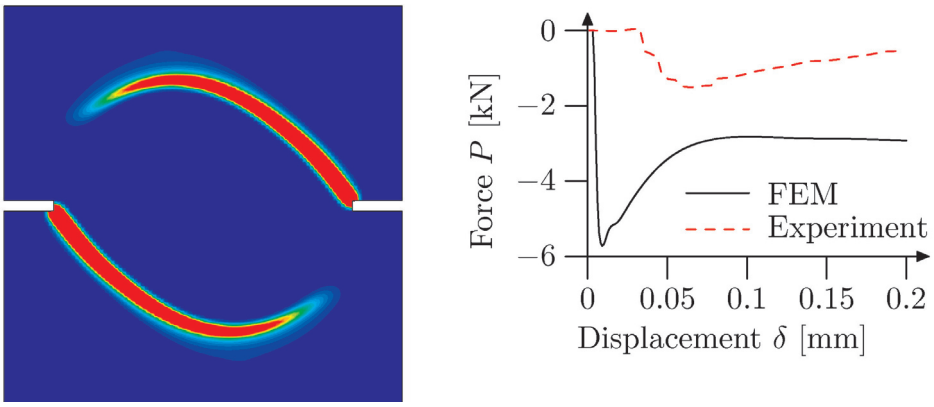


**Fig. 8.** Calculated contour map of parameter $\kappa$ and force-displacement curve at shear force $P_s$ = 29.9 kN using damage mechanics with Eqn. (6)

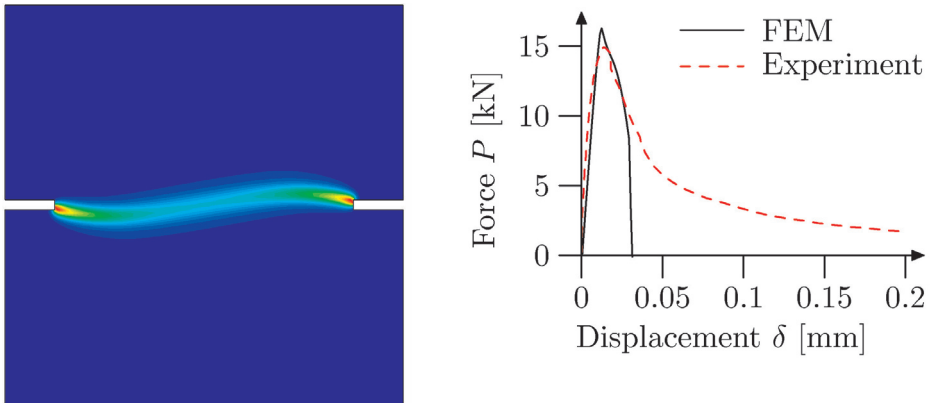


**Fig. 9.** Calculated contour map of parameter κ
and the force-displacement curve at shear force $P_s$ = 5 kN using damage mechanics with Eqn. (8)

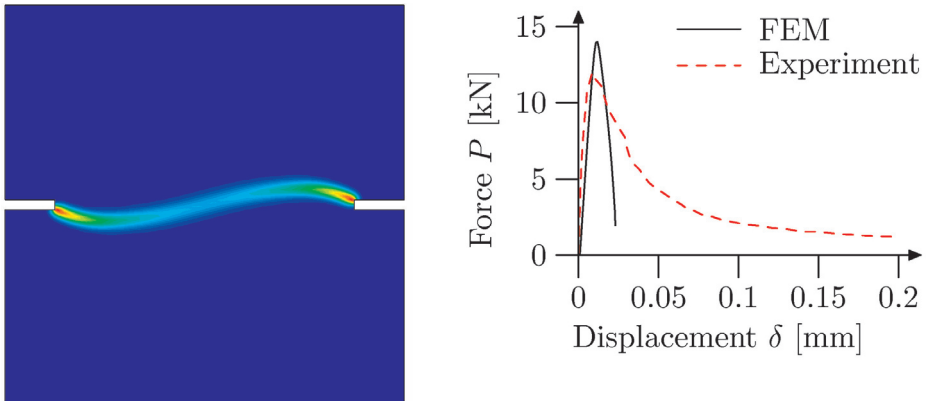


**Fig. 10.** Calculated contour map of parameter κ
and force-displacement curve at shear force $P_s$ = 10 kN using damage mechanics with Eqn. (8)

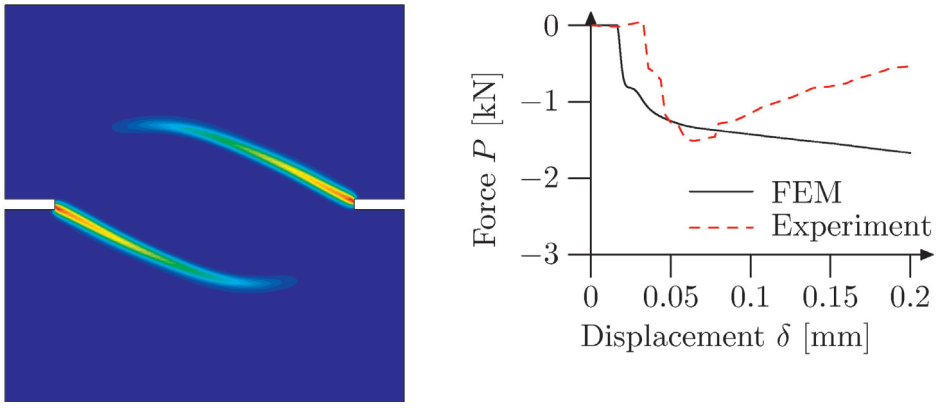


**Fig. 11.** Calculated contour map of parameter κ
and force-displacement curve at shear force $P_s$ = 25.3 using damage mechanics with Eqn. (8)

As a third alternative, a formula proposed by Häußler-Combe and Prochtel (Eqn. (10)) was examined. The following constants were assumed: $\kappa_0 = 6\times10^{-5}$, $\alpha = 0.92$, $\beta = 200$ and $l$ = 2 mm with the parameters $\alpha_1 = 0.08$, $\alpha_2 = 1.16$, $\alpha_3 = 2.0$ and $\gamma = 0.2$. For the lowest shear force, two cracks were obtained (Fig. 12), however at higher shear forces, a third horizontally oriented crack in the middle of the specimen was created (Figs. 13 and 14). The same qualitative outcomes occurred in force-displacement curves: a good agreement at the shear force 5 kN, and an increasing difference at larger values of $P_s$. The maximum calculated shear force was 38.5 kN.

To improve results of the two last series of simulations, some numerical modifications were also investigated. Eqn. (8) was extended to handle a linear dependence of the tensile strength in a tension-compression regime:

$$\tilde{\varepsilon} = \frac{\sigma_1^{eff} - c\left\langle -\sigma_2^{eff} \right\rangle}{E} \tag{21}$$

with $\sigma_1^{eff} > \sigma_2^{eff}$ and a constant $c$. This formulation is equivalent to Eqn. (8) in a tension-tension regime, but it behaves different under tension-compression. The constant $c$ reflects the influence of the principal compression stress.

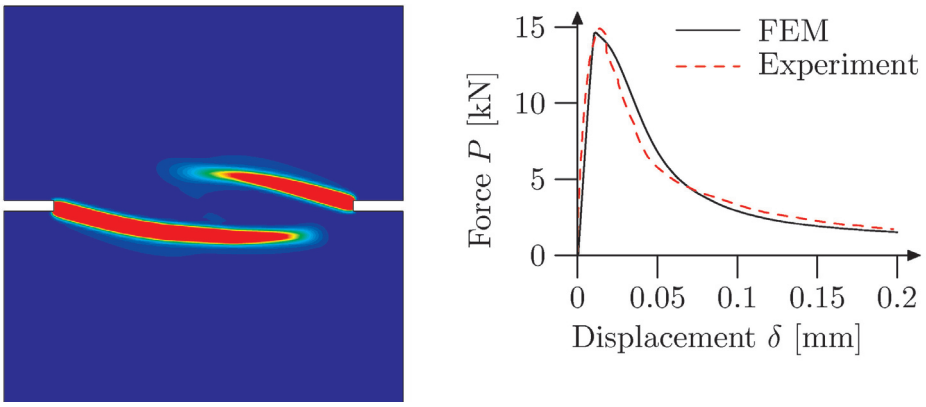


**Fig. 12.** Calculated contour map of parameter κ and the force-displacement curve at shear force $P_s$ = 5 kN using damage mechanics with Eqn. (10)

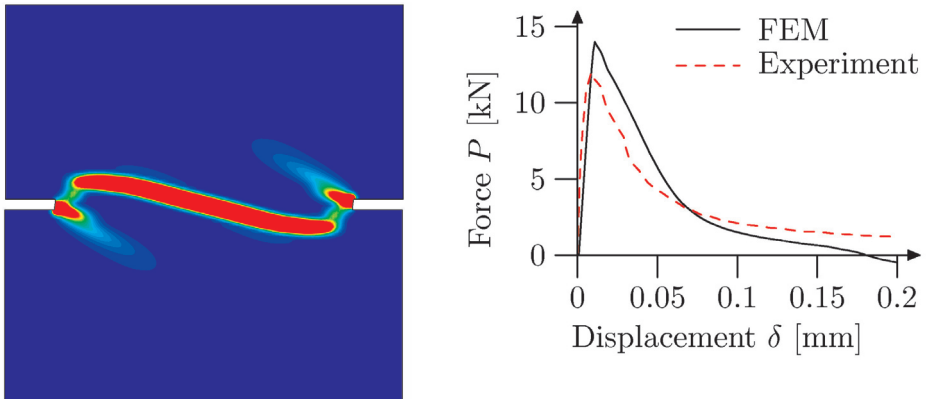


**Fig. 13.** Calculated contour map of parameter κ and force-displacement curve at shear force $P_s$ = 10 kN using damage mechanics with Eqn. (10)

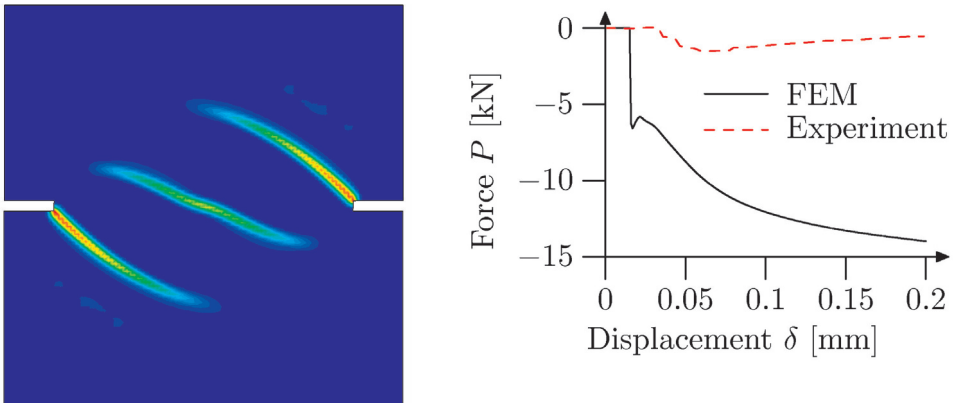


**Fig. 14.** Calculated contour map of parameter κ and force-displacement curve at shear force $P_s$ = 38.5 kN using damage mechanics with Eqn. (10)

With $c$ = 0, Eqn. (8) is recovered. The simulations with a positive constant $c$ did not improve the FE results. The realistic results were solely obtained by defining a negative constant $c$, i.e. by artificially increasing the tensile strength in a tension-compression regime [28].

Finally, some simulations were performed with the improved formula by Häußler-Combe and Prochtel (Eqn. (10)). The most realistic results were achieved by varying the parameters $\alpha_3$ and $\gamma$ and by keeping the parameters $\alpha_1$ and $\alpha_2$ unchanged. An exchange of the parameters $c_3$ and $c_4$ caused an increase of the tensile strength in a tension-compression regime [28].

The simulations with isotropic models indicate that the only way to obtain proper results is to increase artificially the concrete strength in a tension-compression regime (this remark is not related to the both Rankine (Eqn. (8)) and Häußler-Combe and Prochtel (Eqn. (10)) formulas. The modified von Mises definition (Eqn. (6)) already includes this strength increase.

### 5.3. Cohesive elements

The cohesive cracks were described by the tensile strength $f_t$ = 2.2 MPa and the parameters $\eta$ = 0.0 and $\beta$ = 30 000

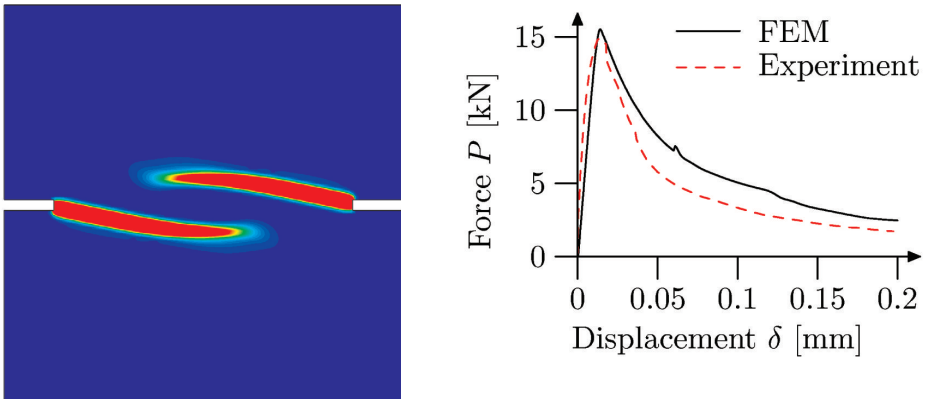


**Fig. 15.** Calculated deformed specimen and force-displacement curve at shear force $P_s$ = 5 kN using cohesive elements

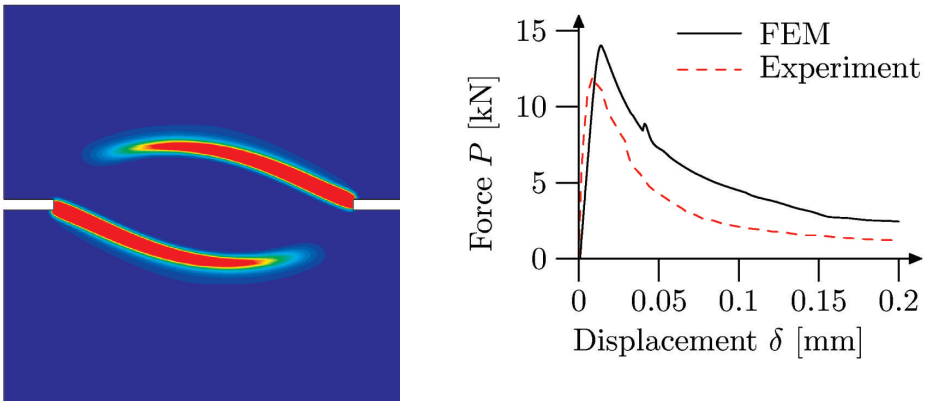


**Fig. 16.** Calculated deformed specimen and force-displacement curve at shear force $P_s$ = 10 kN using cohesive elements

(Section 4.1). The FE mesh with 10184 3-node triangles was used with one integration point. Cohesive elements were placed between elements in the central horizontal region of the specimen. Figures 15 and 16 show the FE results at the shear force $P_s$ equal to 5 kN and 10 kN, respectively. In both cases, a very good agreement was obtained between the experimental and numerical crack patterns and force-displacement curves.

### 5.4. XFEM

The tensile strength was $f_t$ = 3 MPa and the fracture energy $G_f$ = 100 N/m. Two crack starting points were defined near the notch corners. The stress averaging length was $\bar{l}$ = 1 cm. The FE mesh consisted of 3840 3-node triangles with one integration point. Figure 17 shows the numerical results obtained at the shear force $P_s$ = 5 kN. Two inclined cracks were obtained (too highly curved as compared to the experiment). The calculated force-displacement curve indicated unphysical re-hardening caused by a self-locking of both cracks due to their sudden direction change. The crack tips were located at the edges of the earlier cracked elements and the crack evolution was stopped. The FE results at the shear force $P_s$ = 10 kN are presented in Figure 18. Too flat cracks were again calculated. Moreover, a strange jump in

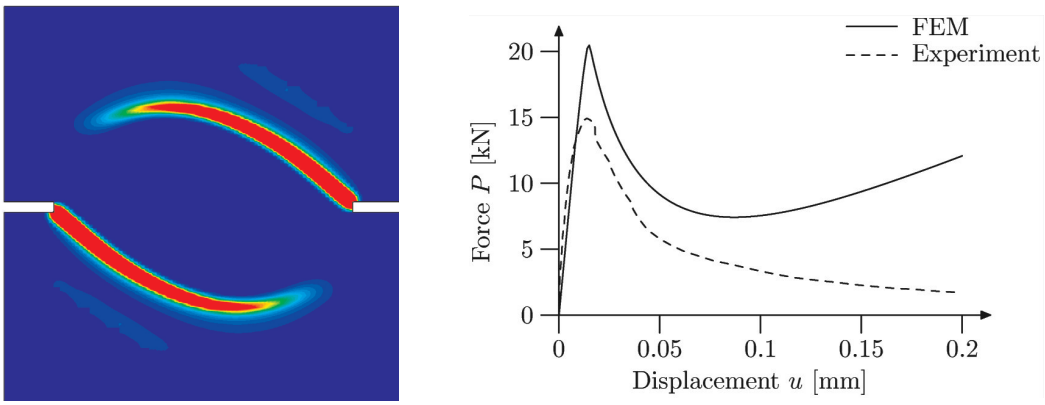


**Fig. 17.** Deformed mesh and force–displacement curve at shear force $P_s$ = 5 kN (displacements were scaled 20 times) using XFEM

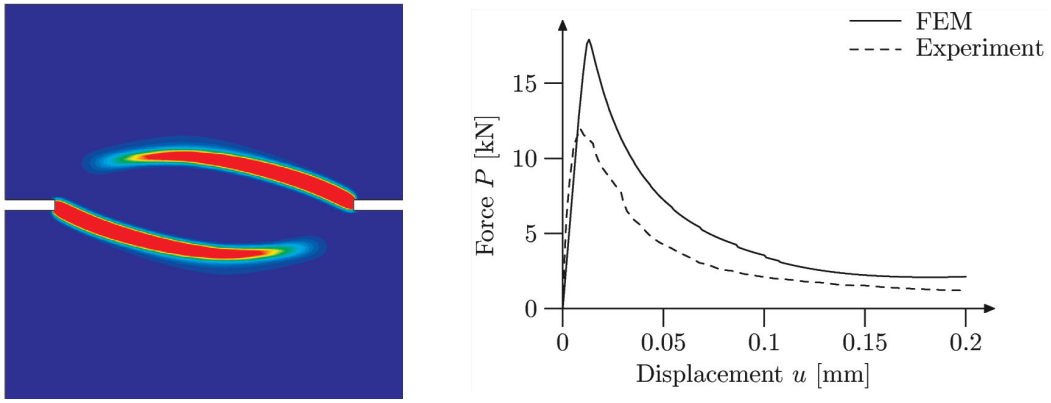


**Fig. 18.** Deformed mesh and force–displacement curve at shear force $P_s = 10$ kN (displacements were scaled 20 times) using XFEM

the crack trajectory was obtained. Despite this fact, a satisfactory agreement was obtained with respect to the force–displacement diagram.

## 6. CONCLUSIONS

Our FE simulations show that both approaches: continuous and discontinuous are able to capture a propagation of curved cracks in concrete elements. In continuum models, a proper choice of a constitutive law is very important for results. An elasto-plastic model with the Rankine criterion is capable of simulating curved cracks in all experimental combinations of tension and shear. Both crack patterns and force-displacement curves are well reproduced. The effectiveness of an isotropic damage constitutive law depends strongly on the equivalent strain measure definition. The wrong results were obtained with the Rankine (Eqn. (8)) and Häußler-Combe–Prochtel (Eqn. (10)) definitions, while other formulas produced acceptable results under condition of an increase of the concrete strength in a tension-compression regime (what is unrealistic). It should be noted that even the use of anisotropic damage models does not guarantee realistic results [13]. The most realistic results within continuum models were achieved by Patzak and Jirasek [12] using a non-local micro-plane model.

For a discontinuous approach, very realistic results were obtained using cohesive elements. An application of XFEM requires, however, further investigations. Although the main items of the experiment were reproduced, the algorithms governing the calculation of a direction of the crack propagation have to be improved to avoid locking in late loading stages. This fact confirms observations done by other researchers [15] that a realistic algorithm to determine the cohesive crack propagation direction is the key point in XFEM formulations. This topic will be deeply investigated in the future. A more advanced description of the constitutive behaviour on the discontinuity based on the effective displacement formulation will be also introduced to XFEM.

**Acknowledgment**

*Research work has been carried out within the project: "Innovative ways and effective methods of safety improvement and durability of buildings and transport infrastructure in the sustainable development" financed by the European Union.*
*The FE-calculations were performed at the Academic Computer Centre in Gdansk TASK.*

## References

[1] Moonen P., Carmeliet J., Sluys L.J. 2008, *A continuous-discontinuous approach to simulate fracture processes*. Philosophical Magazine, 88(28–29), pp. 3281–3298.
[2] Mühlhaus H.-B. 1986, *Scherfugenanalyse bei Granularen Material im Rahmen der Cosserat. Theorie*. Ingenieur Archiv, 56, pp. 389–399.
[3] Pijaudier-Cabot G., Bazant Z.P. 1987, *Nonlocal damage theory*. Journal of Engineering Mechanics ASCE, 113(10), pp. 1512–1533.
[4] De Borst R., Mühlhaus H.-B. 1992, *Gradient-dependent plasticity: Formulation and algorithmic aspects*. International Journal for Numerical Methods in Engineering, 35(3), pp. 521–539.
[5] Melenek J.M., Babuska I. 1996, *The partition of unity finite element method: basic theory and applications*. Computer Methods in Applied Mechanics and Engineering, 139(1–4), pp. 289–314.
[6] Belytschko T., Black T. 1999, *Elastic crack growth in finite elements with minimal remeshing*. International Journal for Numerical Methods in Engineering, 45(5), pp. 601–620.
[7] Moes N., Belytschko T. 2002, *Extended finite element method for cohesive crack growth*. Engineering Fracture Mechanics, 69(7), pp. 813–833.
[8] Wells G.N., Sluys L.J. 2001, *A new method for modelling cohesive cracks using finite elements*. International Journal for Numerical Methods in Engineering, 50(12), pp. 2667–2682.
[9] Nooru–Mohamed M.B. 1992, *Mixed mode fracture of concrete: an experimental research*. Ph.D. Thesis, TU Delft.
[10] Ozbolt J., Reinhardt H.W. 2002, *Numerical study of mixed-mode fracture in concrete*. International Journal of Fracture, 118 (2), pp. 145–161.
[11] Pivonka P., Ozbolt J., Lackner R., Mang H.A. 2004, *Comparative studies of 3D-constitutive models for concrete: application to mixed-mode fracture*. International Journal for Numerical Methods in Engineering, 60 (2), pp. 549–570.
[12] Patzak B., Jirasek M. 2004, *Adaptive resolution of localized damage in quasi-brittle materials*. Journal of Engineering Mechanics ASCE, 2004 (6), pp. 720–732.
[13] Desmorat R., Gatuingt F., Regueneau O. 2007, *Nonlocal anisotropic damage model and related computational aspects for quasi-brittle materials*. Engineering Fracture Mechanics, 74(10), pp. 1539–1560.

[14] Oliver J., Huespe A.E., Samaniego E., Chaves E.W. 2004, *Continuum approach to the numerical simulation of material failure in concrete*. International Journal for Numerical and Analytical Methods in Geomechanics, 28 (7–8), pp. 609–632.
[15] Dumstorff P., Meschke G. 2007, *Crack propagation criteria in the framework of X-FEM-based structural analysis*. International Journal for Numerical and Analytical Methods in Geomechanics, 31(2), pp. 239–259.
[16] Schlangen E., Garboczi E.J. 1996, *New method for simulating fracture using an elastically uniform random geometry lattice*. International Journal of Engineering Science, 34 (10), pp. 1131–1144.
[17] Kozicki J., Tejchman J. 2008, *Modelling of fracture processes in concrete using a novel lattice model*. Granular Matter, 10(5), pp. 377–388.
[18] Tejchman J., Bobiński J. 2011, *Continuous and discontinuous modelling of fracture in concrete using FEM*. Springer (in print).
[19] Hordijk D.A. 1991, *Local approach to fatigue of concrete*. Ph.D. Thesis, TU Delft.
[20] De Vree J.H.P., Brekelmans W.A.M., van Gils M.A.J. 1995, *Comparision of nonlocal approaches in continuum damage mechanics*. Computers and Structures, 55 (4), pp. 581–588.
[21] Jirasek M. 2004, *Non-local damage mechanics with application to concrete*. Revue a francaise de genie civil, 8 (5–6), pp. 683–707.
[22] Häussler-Combe U., Prochtel P. 2005, *Ein dreiaxiales Stoffgesetz fur Betone mith normaler und hoher Festigkeit*. Beton- und Stahlbetonbau, 100 (1), pp. 52–62.
[23] Hsieh S.S., Ting E.C., Chen W.F. 1982, *A plasticity-fracture model for concrete*. International Journal of Solids and Structures, 18 (3), pp. 181–197.
[24] Jirasek M. 2008, *Advanced course on Modeling of Localized Inelastic Deformation*. Lecture Notes, Prague.
[25] Brinkgreve R. 1994, *Geomaterial models and numerical analysis of softening*. Ph.D. Thesis, TU Delft.
[26] Camacho G.T., Ortiz M. 1996, *Computational modelling of impact damage in brittle materials*. International Journal of Solids and Structures, 33(20–22), pp. 2899–2938.
[27] Wells G. 2001, *Discontinuous modelling of strain localisation and failure*. Ph.D. Thesis, TU Delft.
[28] Bobinski J., Tejchman J. 2010, *Continuous and discontinuous modeling of cracks in concrete elements*. Computational Modelling of Concrete Structures Euro-C.